Coupling of Lattice Boltzmann and Finite Element Methods for Fluid-Structure Interaction Application

Y. W. Kwon
Department of Mechanical & Astronautical Engineering,
Naval Postgraduate School,
Monterey, CA 93943

In order to analyze the fluid-structure interaction between a flow and a flexible structure, an algorithm was presented to couple the lattice Boltzmann method (LBM) and the finite element method (FEM). The LBM was applied to the fluid dynamics while the FEM was applied to the structural dynamics. The two solution techniques were solved in a staggered manner, i.e., one solver after another. Continuity of the velocity and traction was applied at the interface boundaries between the fluid and structural domains. Furthermore, so as to make the fluid-structure interface boundary more flexible in terms of the computational modeling perspective, a technique was also introduced for the LBM so that the interface boundary might not coincide with the fluid lattice mesh. Some example problems were presented to demonstrate the developed techniques.
[DOI: 10.1115/1.2826405]

Introduction

Coupled multiphysics problems are very common in real engineering applications. Because of the complexity of the nature, numerical techniques such as the finite element method (FEM), have been applied to coupled problems. There is an extensive amount of literature in the subject field. As a result, it is not the intention of the author to review all of those here. Only some selective work is discussed below. A few of early works in multiphysics applications are found in the literature [1–3]. Among the coupled problems, fluid-structure interaction (FSI) is one of the common applications. FSI examples include, but not limited to, flow over aircraft wing, bridge, and building structures; underwater explosion in interaction with submerged structures [4–6]; flow inside pipes; blood flow in artery; flow over a bundle of pipes; vibration of turbine and compressor blades, etc. As a result, numerical techniques have been also developed for FSI problems. Some of them used FEM for both fluid and structure calculations [7–10], and some others used coupled FEM and the boundary element method [11,12]. Most of those studies considered potential flow for FSI. Viscous flow was considered in blood flow [13,14] using FEM.

The lattice Boltzmann method (LBM) has been developed and applied to fluid flow applications since late 1980s [15–19]. The technique was proved very efficient and powerful for such applications. For example, problems such as multiphase flows [20,21], turbulent flow [22], and thermal flow [23] could be handled effectively using the LBM. On the other hand, the FEM has been utilized dominantly for structural applications. However, to the best knowledge of the author, there was no effort to couple the two techniques to solve the fluid and flexible structure interaction problems. An application of the LBM to FSI was the case with flow around rigid structures as appeared in artificial heart-valve geometries [24]. As a result, this paper presents a technique for coupling of the LBM for the fluid domain and the FEM for the flexible structural domain. In addition, in order to make the fluid-structure interface boundary more flexible in terms of the computational modeling perspective, a technique was also introduced for the LBM so that the interface boundary might not coincide with the fluid lattice mesh. The following sections describe the development of the LBM and treatment of general fluid-structure boundaries. Then, the coupling technique between LBM and FEM is presented. Finally, some numerical examples are presented to demonstrate the coupled technique, and the summary is followed.

Contributed by the Pressure Vessel and Piping Division of ASME for publication in the JOURNAL OF PRESSURE VESSEL TECHNOLOGY. Manuscript received July 31, 2006; final manuscript received December 20, 2006; published online January 8, 2008. Review conducted by F. W. Brust. Paper presented at the 2006 ASME Pressure Vessels and Piping Conference (PVP2006), Vancouver, British Columbia, Canada, July 23–27, 2006.

Lattice Boltzmann Method

This section describes the lattice Boltzmann technique. This technique was originated from lattice gas (LG) automata [25], which are discrete particle kinetics based on discrete time and lattice spaces. The evolution equation for the LG automata is expressed as

$$f_i(\mathbf{x}+\mathbf{e}_i\Delta t, t+\Delta t) - f_i(\mathbf{x},t) = \Omega_i(f(\mathbf{x},t)) \quad (i=0,1,\ldots,n) \quad (1)$$

where $f_i(\mathbf{x},t)$ denotes the number of particles at the lattice site $\mathbf{x}$ and time t, which move along the ith lattice direction with the discrete local particle velocity $\mathbf{e}_i$. Furthermore, Δt is the time increments, and Ω_i is the collision operator for the rate of change of f_i resulting from collision, and it depends only on the local value of $f_i(\mathbf{x},t)$.

In the equation, the local particle velocity is discrete in the given lattice. For example, for a 2D lattice, as shown in Fig. 1, the velocities for the nine possible directions are

$$\mathbf{e}_i = \begin{cases} (0,0) & i=0 \\ c_s(\cos\{(i-1)\pi/2\}, \sin(\{i-1)\pi/2\}) & i=1,2,3,4 \\ \sqrt{2}c_s(\cos\{(i-1)\pi/2+\pi/4\}, \sin\{(i-1)\pi/2+\pi/4\}) & i=5,6,7,8 \end{cases} \quad (2)$$

where c_s is the lattice speed of sound. For the BGK model [26], the collision operator is expressed as

$$\Omega_i = -\frac{1}{\tau}(f_i - f_i^{\mathrm{eq}}) \quad (3)$$

where τ is the relaxation time and f_i^{eq} denotes the local equilibrium distribution. This local equilibrium is expressed as

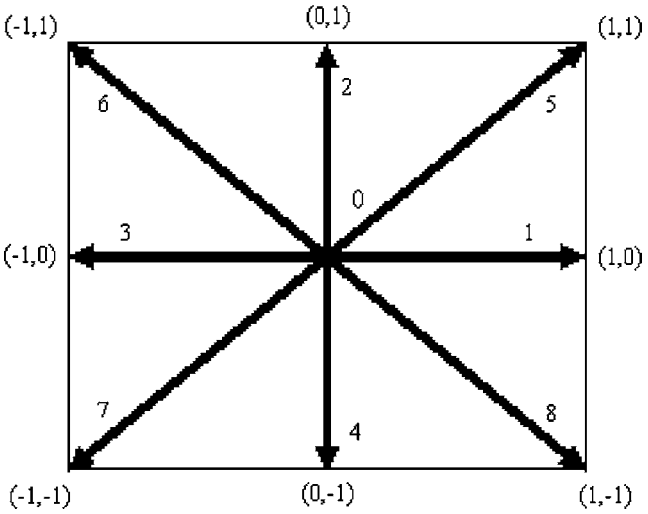

Fig. 1 2D lattice with nine points showing discrete velocity vectors

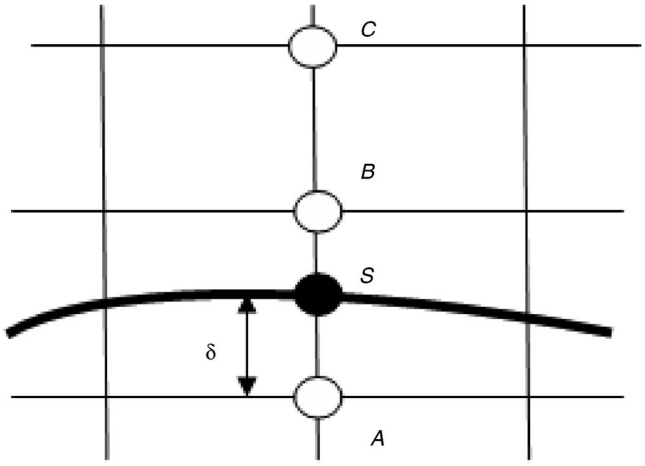

Fig. 2 Structural boundary shown as the bold line with node *S* is located between two fluid lattice Points *A* and *B*. While Point *B* is a real fluid lattice, Point *A* is a fictitious lattice because it is located inside the structure.

$$f_i^{\mathrm{eq}} = pw_i\left[1 + \frac{\mathbf{v}\cdot\mathbf{e}_i}{c_s^2} + \frac{(\mathbf{v}\cdot\mathbf{e}_i)^2 - c_s^2\mathbf{v}\cdot\mathbf{v}}{2c_s^4}\right] \tag{4}$$

in which ρ is the fluid density, and $\mathbf{v}$ is the fluid velocity. In addition, w_i is the weighting parameter for each velocity direction, and it is given below for the 2D lattice shown in Fig. 1:

$$w_i = \begin{pmatrix} 4/9 & i=0 \\ 1/9 & i=1,2,3,4 \\ 1/36 & i=5,6,7,8 \end{pmatrix} \tag{5}$$

The fluid density ρ and momentum $\rho\mathbf{v}$ are expressed as

$$\rho = \sum_i f_i \tag{6}$$

and

$$\rho\mathbf{v} = \sum_i f_i\mathbf{e}_i \tag{7}$$

Furthermore, the fluid pressure p and the kinematic viscosity v are expressed as

$$p = \rho c_s^2 \tag{8}$$

and

$$\nu = c_s^2(\tau - 1/2) \tag{9}$$

General Boundary Treatment in Lattice Boltzmann Method

For FSI problems, the boundary moves as a function of time. If the structural movement is small, the present lattice mesh can be used for the subsequent calculation. On the other hand, if the structural motion is large so that there is a significant change in the fluid-structure interface boundary, the fluid-structure interface boundary will not coincide with the previous fluid lattice mesh. In this case, the LBM lattice needs to be updated. This is a cumbersome and time consuming process. The remeshing may result in an irregular lattice and also affect the accuracy of the LBM solution, even though the irregular lattice could be treated using the finite volume approach of LBM [27,28]. As a result, this section discusses how to treat the case when the FSI boundary does not coincide with the lattice mesh in order to avoid remeshing the lattice.

Figure 2 shows the lying between two neighboring lattice points. In the figure, open circles denote the lattice points while the solid circle indicates the structural node at the fluid-structure interface boundary. The lattice Point B is a real fluid lattice while Point A is a fictitious lattice point because it is inside the structure. Let the distance from one lattice Point A to the structural node S be δ $(0<\delta<1)$ with the normalized lattice spacing of 1. Then, f_i^S is interpolated as

$$f_i^S = (1-\delta)f_i^A + \delta f_i^B \tag{10}$$

where superscript A and B indicate the two lattice points in Fig. 2. From this equation, we obtain

$$f_i^A = (f_i^S - \delta f_i^B)/(1-\delta) \tag{11}$$

If f_i^S is set to zero, then

$$f_i^A = -\delta f_i^B/(1-\delta) \tag{12}$$

Using these approximations, the fluid-structure interface can be handled while it moves between any two neighboring lattice points of the fluid domain. On the other hand, the pressure at the fluid-structure interface is computed from the extrapolation of the fluid pressure as below:

$$p^S = (2-\delta)p^B + (\delta - 1)p^c \tag{13}$$

This pressure equation was derived from a linear extrapolation of pressures at the lattice Points B and C in Fig. 2.

Coupling of Lattice Boltzmann Method and Finite Element Method

One of the boundary conditions at the fluid-structure interface is given as

$$\mathbf{v} = \frac{\partial\mathbf{u}}{\partial t} \tag{14}$$

where $\mathbf{u}$ is the structural displacement vector at the fluid-structure interface boundary and this equation states the continuity of velocity at the interface boundary assuming no slip condition. Furthermore, the continuity of traction at the fluid-structure boundary is expressed as

$$\sigma_{kl}^f n_l = \sigma_{kl}^s n_l \tag{15}$$

in which σ_{kl}^f is the stress tensor in fluid, which is computed as

$$\sigma_{kl}^{f} = -p\delta_{kl} + \mu(\mathbf{v}_{k,l} + \mathbf{v}_{l,k}) \tag{16}$$

σ_{kl}^{s} is the stress at the structure wall, and n_l is the normal unit vector at the interface. In Eq. (16), p is pressure, and μ is the viscosity.

Coupling of LBM to FEM for FSI applications was undertaken in the staggered manner. In other words, the LBM was applied to the fluid domain using the velocity boundary conditions obtained from the FEM at the fluid-structure interface. Then, the fluid traction was computed from the LBM at the fluid-structure boundary. The traction was applied to the structural finite element analysis. This solution cycle continued until the solutions for the fluid and structure became compatible at the interface boundaries.

A procedure to apply the fluid-structure interface velocity boundary condition to the LBM is described below. There is no unique way to apply the structural velocity to the fluid because the LBM does not have the explicit fluid velocity as an unknown variable. In order to find proper $f_i(\mathbf{x},t)$ at the fluid interface, Eq. (7) was used along with the ratios of weight factors shown in Eq. (5). First of all, the so-called bounce-back scheme was applied to the fluid-structure boundary lattice points of the LBM. This means that when a particle distribution hits a boundary lattice point, the particle distribution scatters back to the node it came from. Then, the local particle distribution f_i was further modified as follows to maintain the velocity continuity at the fluid-structure boundary. Let $\dot{u}_x$ and $\dot{u}_y$ be the structural velocity components along the x and y axes at the fluid-structure interface. The particle distribution is revised as follows:

$$f_2 \leftarrow f_2 + \dot{u}_x/3$$

$$f_3 \leftarrow f_3 + \dot{u}_y/3$$

$$f_4 \leftarrow f_4 - \dot{u}_x/3$$

$$f_5 \leftarrow f_5 - \dot{u}_y/3$$

$$f_6 \leftarrow f_6 + \dot{u}_x/12 + \dot{u}_y/12$$

$$f_7 \leftarrow f_7 - \dot{u}_x/12 + \dot{u}_y/12$$

$$f_8 \leftarrow f_8 - \dot{u}_x/12 - \dot{u}_y/12$$

$$f_9 \leftarrow f_9 + \dot{u}_x/12 - \dot{u}_y/12 \tag{17}$$

By doing so, the local fluid mass was conserved at the lattice points lying at the fluid-structure interface and the velocity continuity condition was enforced between the fluid and structure.

Another way to apply the fluid-structure interface velocity to the LBM is described below. In this approach, the bounce-back scheme is not applied to the interface lattice points. Instead, let $\Delta\dot{u}_x$ and $\Delta\dot{u}_y$ be the x and y components of the velocity difference between structure and fluid at the interface. Then, the particle distribution is revised as follows:

$$f_2 \leftarrow f_2 + \Delta\dot{u}_x/3$$

$$f_3 \leftarrow f_3 + \Delta\dot{u}_y/3$$

$$f_4 \leftarrow f_4 - \Delta\dot{u}_x/3$$

$$f_5 \leftarrow f_5 - \Delta\dot{u}_y/3$$

$$f_6 \leftarrow f_6 + \Delta\dot{u}_x/12 + \Delta\dot{u}_y/12$$

$$f_7 \leftarrow f_7 - \Delta\dot{u}_x/12 + \Delta\dot{u}_y/12$$

$$f_8 \leftarrow f_8 - \Delta\dot{u}_x/12 - \Delta\dot{u}_y/12$$

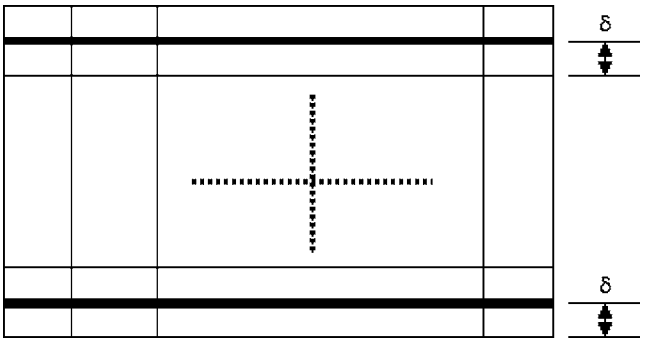

Fig. 3 Poiseuille flow in a channel. The bold lines denote rigid boundaries located between the fluid lattice points.

$$f_9 \leftarrow f_9 + \Delta\dot{u}_x/12 - \Delta\dot{u}_y/12 \tag{18}$$

Comparing the two different approaches using numerical examples, both techniques resulted in quite comparable solutions.

When the traction was computed from the LBM using Eq. (16), then the finite element analysis is conducted using the following equation:

$$[\mathbf{M}]\{\ddot{\mathbf{u}}\} + [\mathbf{C}]\{\dot{\mathbf{u}}\} + [\mathbf{K}]\{u\} = \{\mathbf{F}\} + \{\mathbf{P}\} \tag{19}$$

where $[\mathbf{M}]$, $[\mathbf{C}]$, and $[\mathbf{K}]$ are the finite element mass, damping, and stiffness matrices, respectively. $\{\mathbf{u}\}$ is the nodal displacement vector, and the superimposed dot denotes the temporal derivative. Furthermore, $\{\mathbf{F}\}$ is the external force vector, and $\{\mathbf{P}\}$ is the force vector resulting from the fluid-structure interaction as expressed below:

$$\{\mathbf{P}\} = \sum \int_{\Gamma_{\text{int}}} [\mathbf{N}]^T \{\mathbf{f}\} d\Gamma \tag{20}$$

Here, $[\mathbf{N}]$ is the matrix composed of finite element shape functions over the interface element boundary Γ_{int}, and $\{\mathbf{f}\}$ is the traction vector. The summation is over the total number of finite element boundaries at the fluid-structure interface. For numerical time integration of Eq. (19), the Newmark [29] method was selected because it is an unconditionally stable technique so that the time step size could be determined from the LBM analysis.

Numerical Results

First of all, we consider the case where the fluid-structure interface boundary does not coincide with the fluid lattice points, as shown in Fig. 3. This example is a flow between two rigid panels. However, the rigid panels are located between fluid lattice points as shown in the figure, where δ is the distance of the rigid boundary from the neighboring lattice points. The bold lines indicate the rigid panels. The lattice points between the bold lines are the real fluid lattices. Because this is the Poiseuille flow problem, the LBM solutions are compared to the analytical solution to check the validity of the model. Different δ values in Fig. 3 were selected and their LBM solutions were plotted with the analytical solution in Fig. 4. All velocities and the channel distance in the figure were normalized. As seen in the figure, the LBM velocity profiles match well with the analytical velocity for different δ values.

The next example is illustrated in Fig. 5. As shown in the figure, this example case replaced the rigid bottom plate of the previous example by a flexible structure whose beam flexural rigidity is 833. The normalized transverse displacement at the center of the flexible beam is plotted in Fig. 6 for two different δ values of Fig. 3. The two cases resulted in almost the same displacements as seen in the figure. The results show that the proposed algorithm to treat the fluid-structure interface boundary not coinciding with the fluid lattice worked properly.

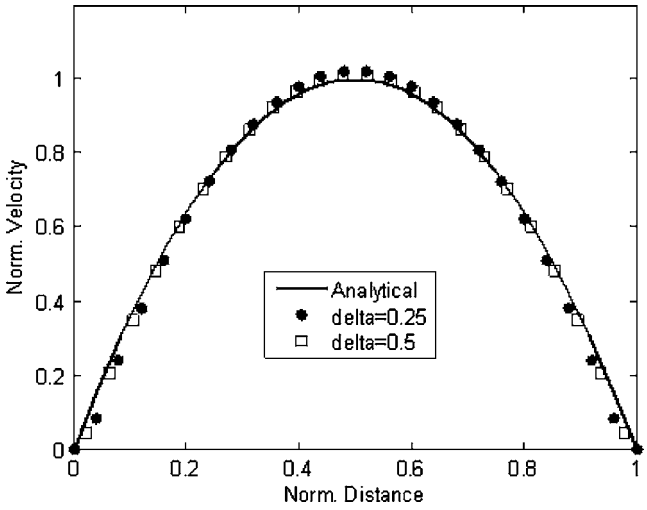

Fig. 4 Normalized velocity distribution for Poiseuille flow with different δ values in Fig. 3

The next example is illustrated in Fig. 7. This example has a slanted flexible structure at the bottom side of the flow channel. The same material properties as before were used for this example. The transverse displacement at the center of the slanted beam is plotted in Fig. 8 as well as its velocity. As time goes, the

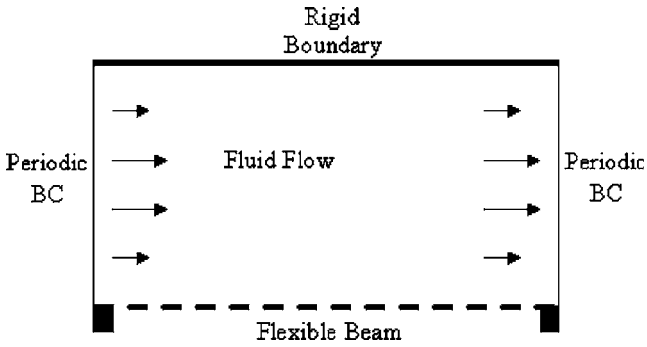

Fig. 5 Flow between a rigid boundary and a flexible beam. The left and right sides have the periodic flow boundary condition.

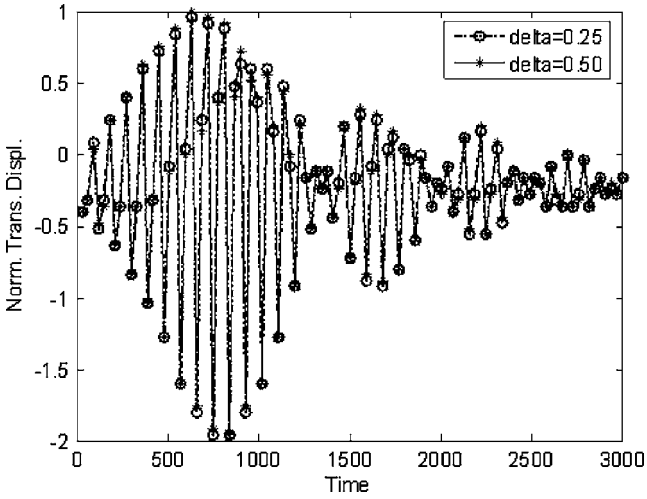

Fig. 6 Time history plot of transverse displacements at the center of the bottom beam of Fig. 5 for two different δ values shown in Fig. 3

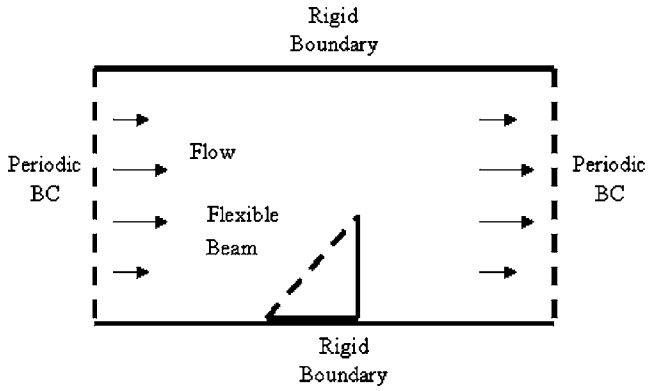

Fig. 7 Flow between two rigid boundaries containing a slanted flexible beam structure inside at the bottom wall

velocity becomes damped out and the transverse displacement approaches to its equilibrium position. Figure 9 shows the flow field at an instant of time. Both flow velocities and the transverse deflection of the flexible beam are shown in the figure.

The last example case to demonstrate a vortex induced vibration was the cavity driven flow inside a flexible container. Figure 10 illustrates the problem. The solid lines indicate the rigid walls while the broken lines denote flexible walls. The selected flow

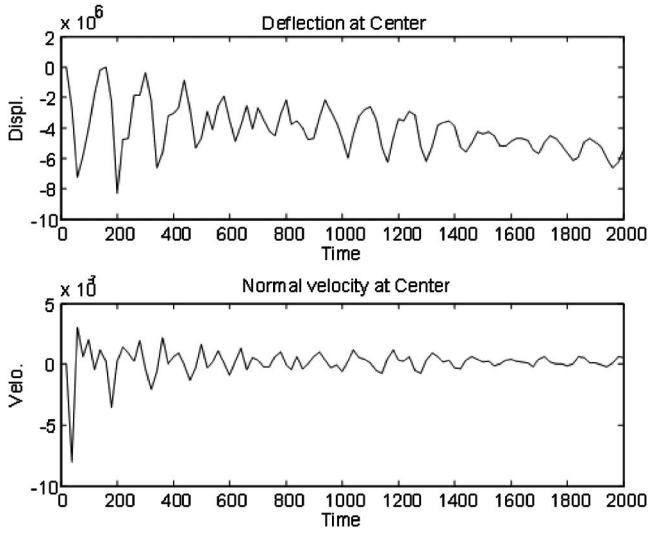

Fig. 8 Transverse displacement and velocity versus time at the center of the flexible beam shown in Fig. 7

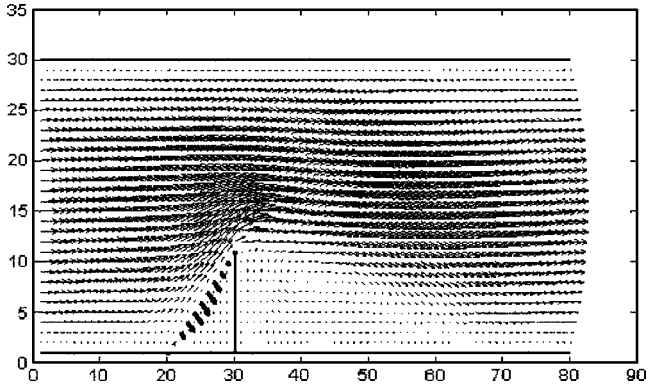

Fig. 9 Plot of the fluid velocity and the structural displacement at an instant of time

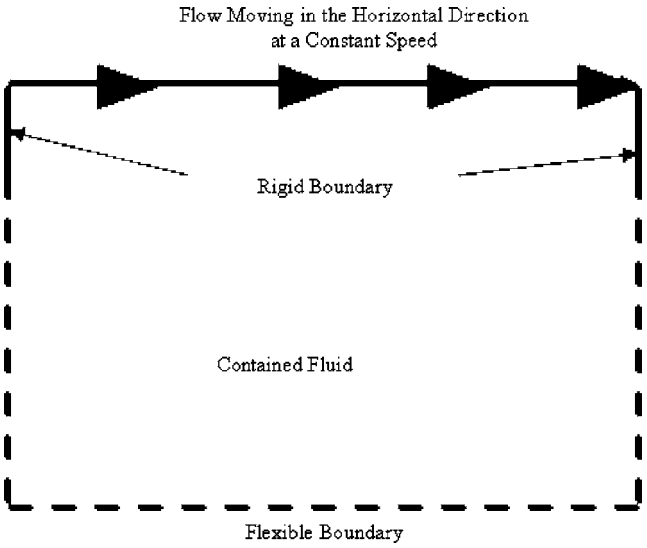

Fig. 10 Cavity driven flow inside a flexible container. The flexible walls are denoted by a broken line.

field lattice size was 25×25. As vortex flow occurs inside the container, the container wall starts to vibrate. The displacements at the center of the bottom side of the container are plotted in Fig. 11 as a function of the normalized time. Both horizontal (i.e., longitudinal) and vertical (i.e., transverse) displacements at that location were plotted. In addition, the flow velocity plot as well as the structural displacement plot are shown in Fig. 12 at a given instant. The transverse displacement of the bottom wall is much smaller than those of the sidewalls so that the former is not shown clearly in the figure.

Summary

A technique was presented to couple the LBM and FEM for FSI applications so that the well-known merits of both techniques could be exploited. For example, LBM is useful to model complex fluid flows while FEM has reached maturity for structural dynamics including nonlinear behaviors. Furthermore, a scheme was also introduced to treat fluid-structure interface boundaries not coinciding with the fluid lattice mesh so that remeshing could be avoided or at least minimized. Some numerical examples were presented to demonstrate the developed techniques. The examples showed the usefulness of the coupled techniques.

An extension of the present technique for 3D cases with more practical applications will be discussed in a subsequent publication. Stability and error analysis will be also conducted in a future study.

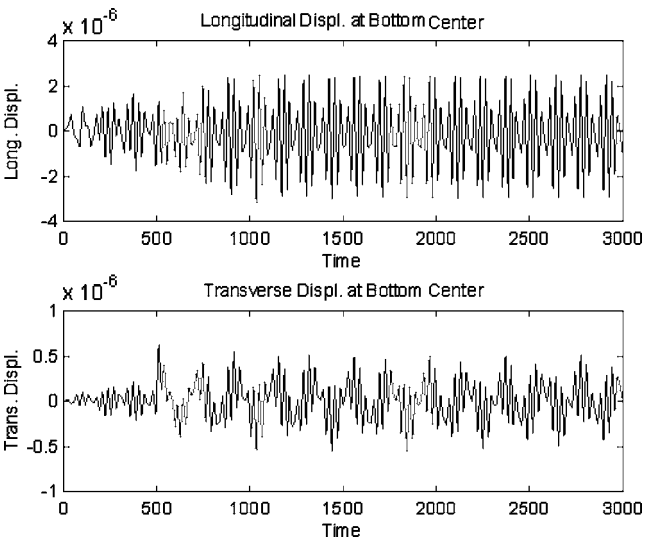

Fig. 11 Time-history plot of longitudinal and transverse displacements of the container at the center of the bottom wall

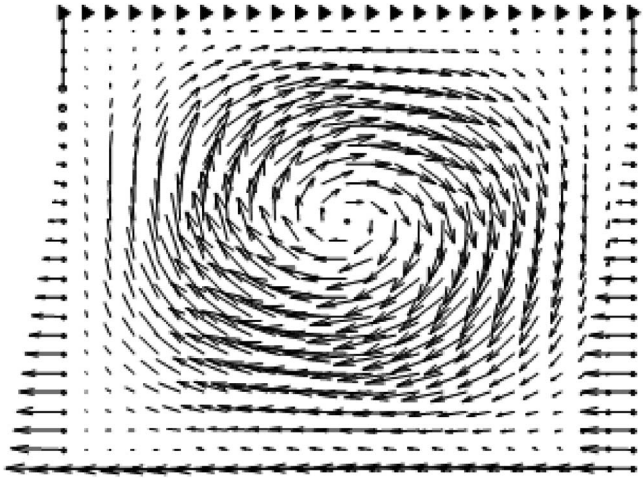

Fig. 12 Plot of fluid velocity and structural displacement of the case shown in Fig. 10 at an instant

References

[1] Zienkiewicz, O. C., and Newton, R. E., 1969, "Coupled Vibration of a Structure Submerged in a Compressible fluid," *Proceedings of International Symposium on Finite Element Techniques*, Stuttgart, May, 1–15.
[2] Zienkiewicz, O. C., Onate, E., and Heinrich, J. C., 1981, "A General Formulation for Coupled Thermal Flow of Metals Using Finite Elements," Int. J. Numer. Methods Eng., **17**, pp. 1497–1514.
[3] Lewis, R. W., Bettess, P., and Hinton, E., 1984, *Numerical Methods in Coupled Systems*, Wiley, Chichester.
[4] Kwon, Y. W., and Fox, P. K., 1993, "Underwater Shock Response of a Cylinder Subjected to a Side on Explosion," Comput. Struct., **48**(4), pp. 637–646.
[5] Kwon, Y. W., Bergensen, J. K., and Shin, Y. S., 1994, "Effect of Surface Coatings on Cylinders Exposed to Underwater Shock," Shock Vib., **1**(3), pp. 637–646.
[6] Kwon, Y. W., and Cunningham, R. E., 1998, "Comparison of USA-DYNA Finite Element Models for a Stiffened Shell Subject to Underwater Shock," Comput. Struct., **66**(1), pp. 127–144.
[7] Newton, R. E., 1980, "Finite Element Study of Shock Induced Cavitation," *ASCE Spring Conference*, Portland, OR.
[8] Zienkiewicz, O. C., Paul, D. K., and Hinton, E., 1983, "Cavitation in Fluid-Structure Response With Particular Reference to Dam Under Earthquake Loading," Earthquake Eng. Struct. Dyn., **11**, pp. 463–381.
[9] Bathe, K. J., Nitikipaiboon, C., and Wang, X., 1995, "A Mixed Displacement-Based Finite Element Formulation for Acoustice Fluid-Structure Interaction," Comput. Struct., **56**, pp. 225–237.
[10] Kwon, Y. W., and McDermott, P. M., 2001, "Effects of Void Growth and Nucleation on Plastic Deformation of Plates Subjected to Fluid-Structure Interaction," ASME J. Pressure Vessel Technol., **123**, PP. 480–485.
[11] Everstine, G. C., and Henderson, F. M., 1990, "Coupled Finite Element/Boundary Element Approach for Fluid-Structure Interaction," J. Acoust. Soc. Am., **87**, pp. 1938–1947.
[12] Giordano, J. A., and Koopmann, G. H., 1995, "State Space Boundary Element-Finite Element Coupling for Fluid-Structure Interaction Analysis," J. Acoust. Soc. Am., **98**, pp. 363–372.
[13] Dubini, G., Pietrabissa, R., and Montevecchi, F. M., 1995, "Fluid-Structure Interaction Problems in Bio-Fluid Mechanics: A Numerical Study of the Motion of an Isolated Particle Freely Suspended in Channel Flow," Med. Eng. Phys., **17**, pp. 609–617.
[14] Tienfuan, K., Lee, L. L., and Wellford, L. C., 1997, "Transient Fluid-Structure Interaction in a Control Valve," ASME Trans. J. Fluids Eng., **119**, pp. 354–359.
[15] MvNamara, G., and Zenetti, G., 1988, "Use of the Boltzmann Equation to Simulate Lattice-Gas Automata," Phys. Rev. Lett., **61**, pp. 2332–2335.
[16] Qian, Y. H., 1993, "Simulating Thermodynamics With Lattice BKG Models," J. Sci. Comput., **8**, pp. 231–241.
[17] Chen, H., 1993, "Discrete Boltzmann Systems and Fluid Flows," Comput. Phys., **7**, pp. 632–637.
[18] Cali, A., Succi, S., Cancelliere, A., Benzi, R., and Gramingnani, M., 1992,

"Diffusion and Hydrodynamic Dispersion With the Lattice Boltzmann Method," Phys. Rev. A, **45**, pp. 5771–5774.
[19] Chen, S., and Doolen, G. D., 1998, "Lattice Boltzmann Method for Fluid Flow," Annu. Rev. Fluid Mech., **30**, pp. 329–364.
[20] Flekkoy, E. G., 1993, "Lattice Bhatnagar-Gross-Krook Models for Miscible Fluids," Phys. Rev. E, **47**, pp. 4247–4257.
[21] Swift, M. R., Orlandini, E., Osborn, W. R., and Yeomans, J. M., 1996, "Lattice Boltzmann Simulations of Liquid-Gas and the Binary Fluid Systems," Phys. Rev. E, **54**, pp. 5041–5052.
[22] Soe, M., Vahala, G., Pavlo, P., Vahala, L., Chen, H., 1998, "Thermal Lattice Boltzmann Simulations of Variable Prandtl Number Turbulent Flows," Phys. Rev. E, **57**, pp. 4227–4237.
[23] Peng, Y., Shu, C., and Chew, Y. T., 2003, "Simplified Thermal Lattice Boltzmann Model for Incompressible Thermal Flows," Phys. Rev. E, **68**, p. 026701.
[24] Krafczyk, M., Tolke, J., Rank, E., and Schulz, M., 2001, "Two-Dimensional Simulation of Fluid-Structure Interaction Using Lattice-Boltzmann Methods," Comput. Struct., **79**, pp. 2031–2037.
[25] Frisch, U., Hasslacher, B., and Pomeau, Y., 1986, "Lattice-Gas automata for the Navier–Stokes Equations," Phys. Rev. Lett., **56**, pp. 1505–1508.
[26] Bhatnagar, P., Bross, E. P., and Krook, M. K., 1954, "A Model for Collision Process in Gases. I: Small Amplitude Processes in Charged and Neutral One-Component System," Phys. Rev., **94**, pp. 511–525.
[27] Peng, G., Xi, H., and Duncan, C., 1998, "Lattice Boltzmann Method on Irregular Meshes," Phys. Rev. E, **58**, pp. R4124–R4127.
[28] Xi, H., Peng, G., and Chou, S.-H., 1999, "Finite-Volume Lattice Boltzmann Method," Phys. Rev. E, **59**, pp. 6202–6205.
[29] Newmark, N. M., 1959, "A Method of Computation for Structural Dynamics," J. Engrg. Mech. Div., **85**, pp. 67–94.